


Coherent and dissipative dynamics of entangled few-body systems of Rydberg atoms

Woojun Lee, Minhyuk Kim, Hanlae Jo, Yunheung Song, and Jaewook Ahn
 Department of Physics, KAIST, Daejeon 305-701, Korea

 (Received 24 January 2019; published 5 April 2019)

Experimentally observed quantum few-body dynamics of neutral atoms excited to a Rydberg state are numerically analyzed. For this, up to five rubidium atoms are trapped with optical tweezers, arranged in various two-dimensional configurations, and excited to the Rydberg $6S$ state in the nearest-neighbor blockade regime. Their coherent evolutions are measured with time-varying ground-state projections and the experimental results are analyzed with a model Lindblad equation with the homogeneous and inhomogeneous dampings determined by systematic and statistical error analysis. The coherent and dissipative dynamics of these entangled systems are successfully reproduced using the given model and external parameters optimally calibrated with the experimental results.

DOI: [10.1103/PhysRevA.99.043404](https://doi.org/10.1103/PhysRevA.99.043404)

I. INTRODUCTION

Neutral atoms have been a promising candidate platform for quantum information science and quantum many-body physics studies [1–5]. They have well-defined energy levels, long coherence, and lifetimes, which are all essential for their usage as qubits in quantum information science [3]. Furthermore, atoms can be controlled as individual quanta [6,7], rather than as a collective ensemble, through the developments in laser cooling and trapping techniques, and these atoms can be easily entangled through Rydberg-state excitation [8–12]. In recent demonstrations, as many as 100 single atoms were arranged with a set of independently controlled optical tweezers [13–19]. With these entangled single-atom systems, Rydberg quantum simulators were constructed, having about 25 to 51 qubits, and used to probe the many-body dynamics of Ising-type or XY quantum spin models across phase transitions [20–22] and also towards thermalization [23].

Rydberg atoms strongly interact with each other due to the high polarizability and large-scale dipoles, compared to the ground-state atoms. The giant dipole-dipole interaction among closely lying Rydberg atoms can shift the resonance of the double excitations out of the range of excitation laser bandwidth, inhibiting the excitations of all other atoms during one is excited. This Rydberg dipole-blockade is of much interest as an effective way to implement entanglements [9,10] and controlled-NOT (C-NOT) gates [11,12] in quantum computation and quantum simulation [20–24].

Precise measurements and control of the quantum evolution of these atoms, particularly in their entanglements, are highly important in quantum simulations [24], in which measured system dynamics are used to reproduce and predict the dynamics of other many-body quantum systems. However, the system dynamics of an entangled many-body system, which are given as a combination of coherent Hamiltonian and dissipative open-system evolution, are vulnerable to environmental errors. In this paper, we present a numerical analysis of experimentally observed quantum few-body dynamics of Rydberg atoms. We first measure the coherent evolutions of up to five rubidium atoms arranged in various two-dimensional

configurations and entangled through Rydberg state excitation, and the measured results are analyzed with a model Lindblad master equation with homogeneous and inhomogeneous dephasings.

The rest of this article is organized as follows. In Sec. II, we provide a brief theoretical model description of the quantum dynamics of Rydberg atomic systems. Experimental setup and procedure are described in Sec. III, before the result in Sec. IV, and possible error sources are discussed in Sec. V. A summary is given in Sec. VI.

II. THEORETICAL DESCRIPTION

We consider N atoms arranged in two-dimensional space and interacted with light near-resonant to a Rydberg state. The Hamiltonian, without dephasings taken into account, is given by

$$\hat{H} = \frac{\hbar}{2} \sum_{j=1}^N \{ \Omega e^{i\phi} |0\rangle_j \langle 1|_j + \Omega e^{-i\phi} |1\rangle_j \langle 0|_j - \Delta \hat{\sigma}_z^{(j)} \} + \sum_{k<l} V_{kl} \hat{n}_k \hat{n}_l, \quad (1)$$

where $\hat{\sigma}_z^{(j)} = |0\rangle_j \langle 0|_j - |1\rangle_j \langle 1|_j$ and $\hat{n}_k = |1\rangle_k \langle 1|_k$ are defined for pseudospinors $|0\rangle = |g\rangle$ (the ground state) and $|1\rangle = |R\rangle$ (the Rydberg state), $\Omega e^{i\phi}$ is the Rabi frequency with phase, Δ is the detuning, and $V_{kl} = -C_6/r_{kl}^6$ is the van der Waals interaction [25] between two Rydberg atoms separated by r_{kl} .

As an exemplary set, we consider six two-dimensional arrangements of $N = 3$ –5 atoms as shown in Fig. 1: (a) triangular three ($N = 3$) atoms arranged at the vertices of an equilateral triangle, (b) a linear arrangement of three atoms, (c) a zigzag arrangement of four atoms, (d) linear four atoms, (e) zigzag five atoms, and (f) linear five atoms. In each configuration, the nearest-neighbor distance is smaller and the next-nearest is larger than the blockade radius [8] (i.e., $r_{\text{n.n.}} < r_B = (|C_6|/\hbar\Omega)^{-1/6} < r_{\text{n.n.n.}}$). In this case, double excitations of any and only neighboring pairs are prohibited almost,

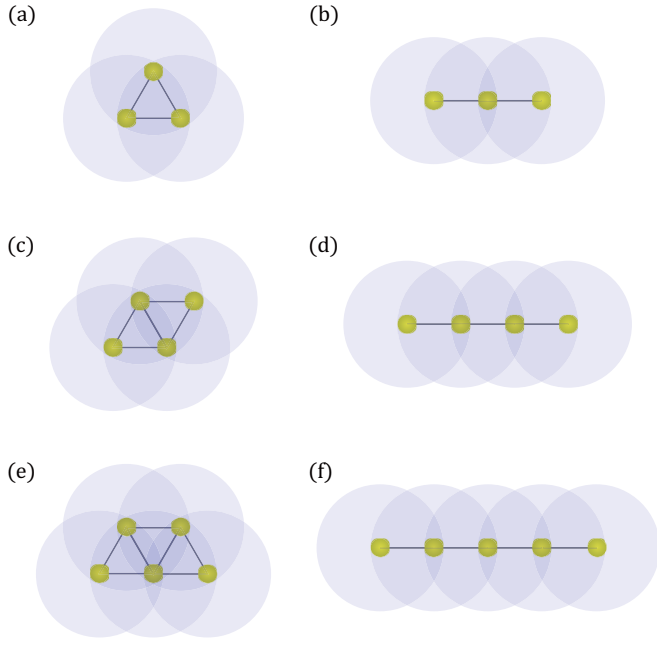


FIG. 1. Atom configurations: (a) triangular three atoms ($r_{12} = r_{23} = r_{13}$); (b) linear three atoms ($r_{12} = r_{23} = r_{13}/2$); (c) zigzag four atoms ($r_{12} = r_{13} = r_{14} = r_{24} = r_{34} = r_{23}/\sqrt{3}$); (d) linear four atoms ($r_{12} = r_{23} = r_{34} = r_{13}/2 = r_{24}/2 = r_{14}/3$); (e) zigzag five atoms; (f) linear five atoms. Each circle represents the radius of Rydberg blockade, which is larger than the nearest-neighbor distance and smaller than the next-nearest-neighbor distance, i.e., $r_{(nn)} < r_R < r_{(n nn)}$.

and this prohibition becomes complete in an approximation of ignoring all the longer-distance interactions. Under this approximation, the quantum dynamics of the triangular three atoms in Fig. 1(a) is a collective Rabi oscillation [26], of which the time evolution is given by

$$|\psi(t)\rangle = a_0(t)|000\rangle + a_1(t)\frac{|100\rangle + |010\rangle + |001\rangle}{\sqrt{3}}, \quad (2)$$

where $|000\rangle$ is the zero-excitation state and the second term is the superposition of singly excited states. Likewise, the dynamics of the linear three atoms in Fig. 1(b) is given in the symmetry basis $\{|000\rangle, |010\rangle, (|100\rangle + |001\rangle)/\sqrt{2}, |101\rangle\}$, the zigzag four atoms in Fig. 1(c) is in $\{|0000\rangle, (|1000\rangle + |0001\rangle)/\sqrt{2}, (|0100\rangle + |0010\rangle)/\sqrt{2}, |1001\rangle\}$, and so on.

Dephasing of a mixed state is in general described by a Lindblad master equation [27–29], which reads

$$\frac{d\rho}{dt} = -\frac{i}{\hbar}[H, \rho] + \mathcal{L}_{\text{ind}}(\rho) + \mathcal{L}_c(\rho), \quad (3)$$

where ρ is a 2^N -by- 2^N density matrix, \mathcal{L}_{ind} and \mathcal{L}_c are the Lindblad superoperators for individual and collective dephasings, respectively, given by

$$\mathcal{L}_{\text{ind}}(\rho) = \sum_{j=1}^N \left(L_j \rho L_j^\dagger - \frac{1}{2} \{L_j^\dagger L_j, \rho\} \right), \quad (4)$$

$$\mathcal{L}_c(\rho) = L_0 \rho L_0^\dagger - \frac{1}{2} \{L_0^\dagger L_0, \rho\}. \quad (5)$$

In Eq. (4), L_j is the Lindblad operator for individual (atom j) dephasing, given by

$$L_j = I^{(1)} \otimes I^{(2)} \cdots \otimes \sqrt{\frac{\gamma_{\text{ind}}}{2}} \sigma_z^{(j)} \cdots \otimes I^{(N)}, \quad (6)$$

where I is the 2-by-2 identity matrix and γ_{ind} is the individual dephasing rate. In Eq. (5), L_0 is the Lindblad operator for collective dephasing, given as a sum of L_j with collective dephasing rate γ_c replacing the individual dephasing γ_{ind} in Eq. (6). As to be explained in Sec. IV, in our experiment, the individual dephasing is mainly caused by the spontaneous emission through intermediate state and the collective dephasing is negligible.

Additionally, the phase ϕ of the Rabi frequency $\Omega e^{i\phi}$ in Eq. (1) changes in time due to the phase noise of Rydberg-state excitation lasers. This phase noise induces apparently a dephasing behavior, as recently discussed in a single-body dephasing model [30]. In the interaction picture, where the phase is eliminated from the Rabi frequency and treated as a detuning, the Hamiltonian $H' = U H U^\dagger - i\hbar U \dot{U}^\dagger$, basis-transformed with phase-rotation $U = \prod_{j=1}^N (|0\rangle_j \langle 0|_j + e^{i\phi(t)} |1\rangle_j \langle 1|_j)$, is given by

$$\hat{H}' = \frac{\hbar}{2} \sum_{j=1}^N \{ \Omega \hat{\sigma}_x^{(j)} - [\Delta + \dot{\phi}(t)] \hat{\sigma}_z^{(j)} \} + \sum_{k<l} V_{kl} \hat{n}_k \hat{n}_l, \quad (7)$$

where $\hat{\sigma}_x^{(j)} = |0\rangle_j \langle 1|_j + |1\rangle_j \langle 0|_j$. The time-dependent detuning is then given by $\Delta(t) = \Delta + \dot{\phi}(t)$, which can be analyzed as a Fourier series, i.e.,

$$\Delta(t) = 2 \int |\tilde{\Delta}(f)| \cos[2\pi f t + \xi(f)] df, \quad (8)$$

with spectral amplitude $|\tilde{\Delta}(f)|$ and spectral phase $\xi(f)$ of $\Delta(t)$. So, when the laser phase noise in repetitive measurements randomizes $\xi(f)$ and induces $\Delta(t)$ fluctuations, an apparent dephasing behavior can appear in the given quantum dynamics.

III. EXPERIMENTAL SETUP AND PROCEDURE

The experimental setup is shown in Fig. 2, which is similar to our earlier reports [14,15,23,31]. In brief, the setup consists of a magneto-optical trap (MOT) for cold rubidium atoms (^{87}Rb), a control system of optical tweezers (far-off resonance dipole traps), and an optical system for Rydberg excitation. Rubidium atoms were first cooled to 30 μK through Doppler and polarization-gradient coolings. During the cooling stage, optical tweezers (of 820-nm wavelength, 1-mK trap-depth, and 1.4- μm diameter) were trapping atoms at pre-determined target sites and the MOT was turned off by shutting off the anti-Helmholtz coils. Typical arrays before rearrangements were about half-filled due to collisional blockade [6]. So, the occupancy or vacancy in each optical tweezer was checked with fluorescence imaging $|5S_{1/2}, F=2\rangle \rightarrow |5P_{3/2}, F'=3\rangle$ by an electron multiplying charge-coupled device (EMCCD). After the occupancy was all checked, unity-filled arrays were then created with reconfiguration of captured atoms [16,31] through two times of the three-step processes of imaging, vacancy-filling, and verification. The six different atom

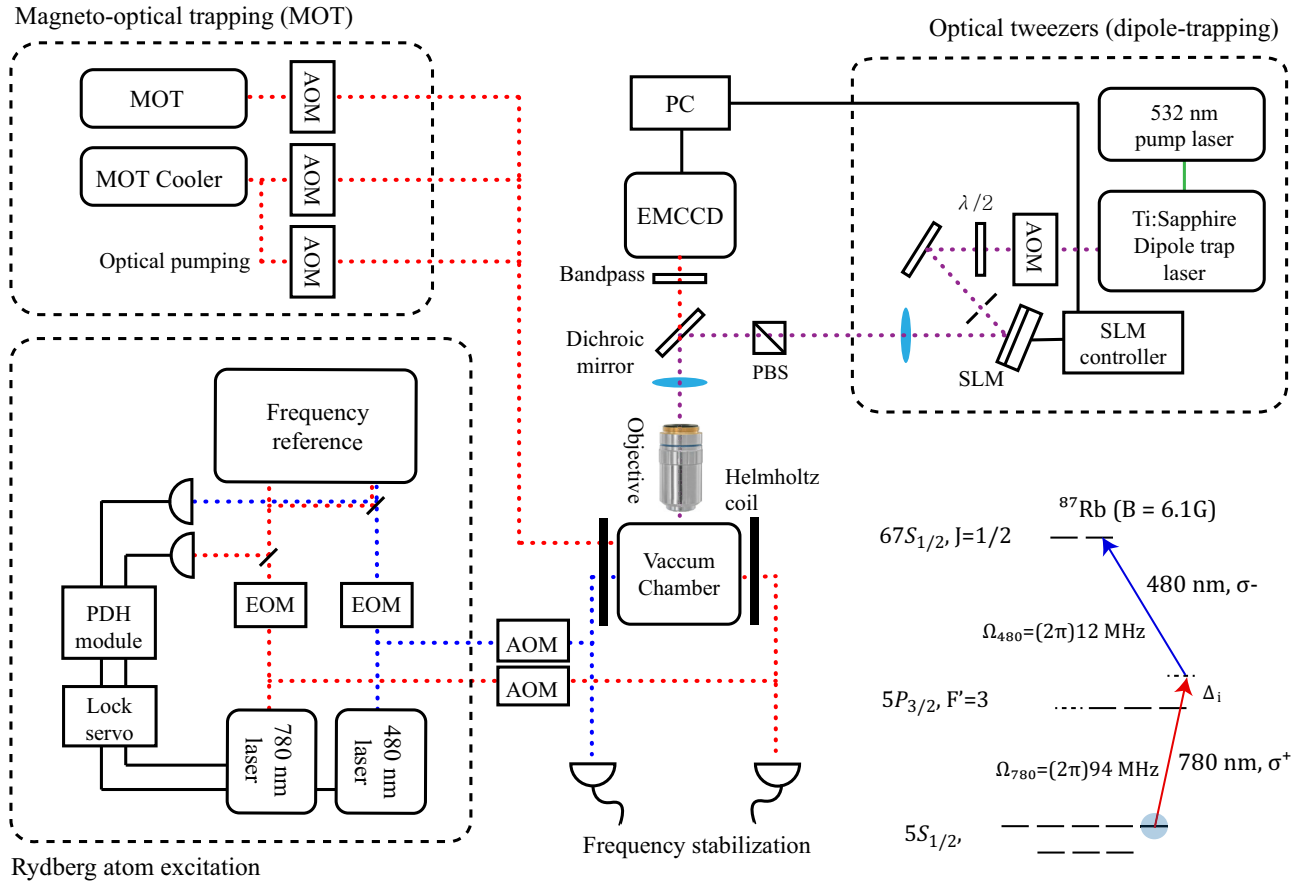


FIG. 2. A schematic diagram of the experimental setup and the energy level diagram for Rydberg-state excitation (AOM: acousto-optic modulator, EOM: electro-optic modulator, PC: personal computer, SLM: spatial light modulator, PBS: polarization beam splitter).

configurations, introduced in Sec. II, were produced, which were linear or zigzag $N = 3, 4$, or 5 atoms.

After a unity-filled atom arrangement was prepared, Rydberg-state excitation was performed through the two-photon transition from $|g\rangle = |5S_{1/2}, F = 2, m_F = 2\rangle$ to $|R\rangle = |67S_{1/2}, m_J = 1/2\rangle$ via off-resonant intermediate state $|m\rangle = |5P_{3/2}, F' = 3, m'_F = 3\rangle$ [32]. We used 780-nm and 480-nm lasers (diode lasers from Toptica), counterpropagating with σ^+ and σ^- polarizations, respectively. The Rabi frequency of the two-photon transition is given by $\Omega = \Omega_{780}\Omega_{480}/(2\Delta_i) = (2\pi)1.0$ MHz, where $\Omega_{780} = (2\pi)94$ MHz and $\Omega_{480} = (2\pi)12$ MHz are the Rabi frequencies of the one-photon transitions ($|g\rangle \rightarrow |m\rangle$ and $|m\rangle \rightarrow |R\rangle$), and $\Delta_i = -(2\pi)560$ MHz is the one-photon detuning of the 780-nm laser from the intermediate transition ($|g\rangle \rightarrow |m\rangle$). The diameters of the 780- and 480-nm lasers were 100 and 10 μm , respectively, so that the atoms in dynamics were under homogeneous Rabi frequencies. The homogeneity was also verified by a set of separate single-atom experiments. The magnitude of Ω_{480} was limited by the maximum laser power. Note that Doppler effect shifts the frequency of the excitation laser, causing detuning of ~ 100 kHz for the atom temperature of 30 μK which is considered small in our experiment.

The phase of the Rabi frequency is $\phi = \phi_{780} + \phi_{480}$, the sum of the phases of the lasers. The frequencies of the lasers were stabilized to a narrow linewidth of $< (2\pi)30$ kHz with

an ultralow expansion (ULE) reference cavity (from Stable Laser Systems). The ULE cavity had a finesse of 15 000 and antireflection coated at the dual wavelengths of 780 and 480 nm. The laser wavelengths were roughly monitored by a wavemeter (HighFinesse WS7-60) within 60 MHz accuracy, and Pound-Drever-Hall (PDH) locking technique (PDH module from Stable Laser Systems and PDD110 from Toptica) was adopted to lock the laser frequencies to the Fabry-Perot signal reflected from the reference cavity, in conjunction with fast lock servos (FALC110 from Toptica).

To suppress the stray E-fields, metallic instruments around the chamber were electrically grounded. The amount of the atom resonance shift was decreased from 16 MHz to 200 kHz, which corresponded to the E-field of 50 to 0.6 mV/cm. Our internal simulations showed a 200 kHz of resonance shift made little effect to the dynamics.

The time sequence of the experimental procedure is summarized in Fig. 3. Before the Rydberg-state excitation, optical pumping to $|g\rangle$ was performed for 2 ms, when the quantization axis was defined with a Helmholtz bias coil ($B = 6.1$ G). Then we turned on the 480-nm laser, turned off the optical tweezers for 3.4 μs to avoid push-out of atoms in the Rydberg states (due to the light-induced potential), and finally turned on the 780-nm laser for Rydberg-state excitation. After the 780-nm laser turn-on with various pulse durations, the optical tweezers were turned back on to recapture the atoms in $|g\rangle$. Whether

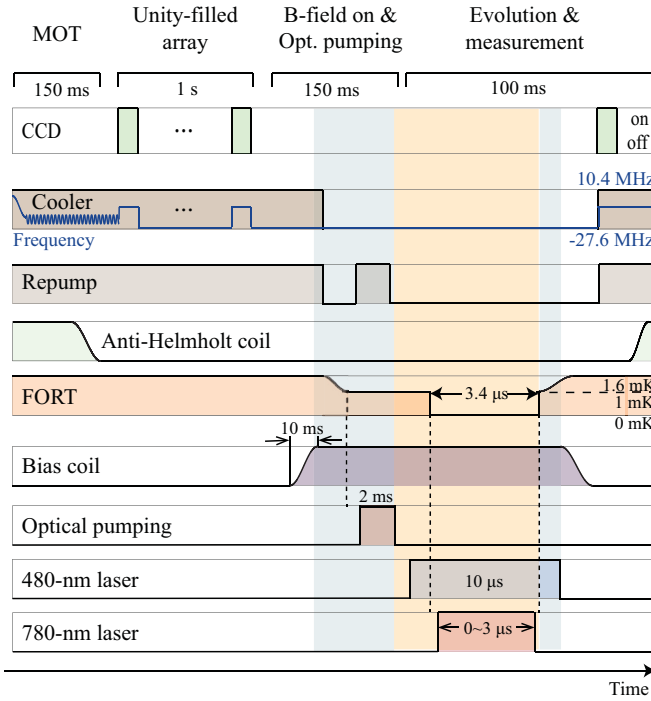


FIG. 3. Experimental procedure: the time sequences of fluorescence imaging, MOT cooling, and repumping, anti-Helmholtz current, far-off resonant trapping (optical tweezers), bias B-field, optical pumping, and Rydberg-state excitation with 480-nm and 780-nm lasers, respectively.

each atom was recaptured or not (a projection measurement to $|g\rangle$) was recorded with the fluorescence imaging through $|5P_{3/2}, F' = 3\rangle$.

IV. RESULTS

Experimentally measured quantum dynamics are summarized in Fig. 4. The results for the total six configurations, $N = 3-5$ atoms in linear or zigzag configuration, are shown in Figs. 4(a) to 4(f), where the Rydberg blockade radius was $r_R = 8.8(3) \mu\text{m}$ and the lattice constant was $d = 6.1(3) \mu\text{m}$. For example, the case of the equilateral triangular three atoms is shown in Fig. 4(a), where the schematic geometry and the image of the atoms are shown in the leftmost column, and the measured probabilities are in the right columns. The time-evolving state probabilities are plotted for the symmetry bases $|000\rangle$ and $(|100\rangle + |010\rangle + |001\rangle)/\sqrt{3}$, as in Eq. (2). The scan range of the quantum evolution was $0-3 \mu\text{s}$ with a time step of $0.1 \mu\text{s}$ (total 31 data points with 150 repetitive measurements). Similarly, the case of three atoms in the linear configuration is shown in Fig. 4(b), where the constituent symmetry bases are $|000\rangle$, $|010\rangle$, $(|100\rangle + |001\rangle)/\sqrt{2}$, and $|101\rangle$. The remaining configurations are also represented, with the probability measurements for the corresponding sets of symmetry bases.

In comparison, numerical calculations were performed with Eqs. (3) and (7), taking into account the contributions of experimental and measurement errors. As to be discussed in Sec. V, major error sources are: (a) the spontaneous decay from $|R\rangle$ to $|g\rangle$, (b) optical-tweezer atom loss, (c) leakage to

intermediate state, and (d) laser noise. Table I summarizes the experimental uncertainties related to these error sources. The noises in laser intensity and phase were $\delta I/I = 3\%$ and $|\Delta| = 0.4\Omega$, respectively. The position uncertainty of the optical tweezers was $\delta r/r = 5\%$. The measurement uncertainty was $\delta P = 3\%$, mainly from the spontaneous emission from $|R\rangle$ to $|g\rangle$ and also atom escapes from optical tweezers.

Each solid line in Fig. 4 represents the calculation. We used a numerical fitting with two parameters, $\alpha \equiv \Omega/\Omega_0$ and $\beta \equiv |\tilde{\Delta}(f)|/|\tilde{\Delta}(f)|_0$, where Ω_0 and $|\tilde{\Delta}(f)|_0$ are the references retrieved from single-atom experiments. After randomization with $\xi(f)$ in Eq. (8), we obtain $(\alpha, \beta) = (0.94, 3.1 \text{ dB})$, $(1.04, 0.0 \text{ dB})$, $(0.96, 0.0 \text{ dB})$, $(1.02, 1.3 \text{ dB})$, $(0.96, 0.6 \text{ dB})$, and $(0.96, 3.1 \text{ dB})$ for the six configurations, respectively. The dashed and dot-dashed lines in each figure are the calculations with $\delta\beta = \pm 3 \text{ dBm}$ shifts, respectively, from the above values. To estimate how well the experimental data are replicated by the model fitting, R^2 values are calculated, which are the proportion of the measured behaviors explained by the model. With the optimal fitting conditions of (α, β) , we get $R^2 = 0.90(1)$ (e.g., for $N = 3$ cases) and this value gradually decreases below 0.6 when $\Delta\alpha = 20\%$ or $\Delta\beta = \pm 3 \text{ dB}$. Note that calculations without the phase noise taken into account give a similar R^2 values below 0.6.

V. DISCUSSIONS

Deviations from ideal dynamics, for example, a simple two-state oscillation for the triangular three atoms in Fig. 3(a), are attributed to mainly four different physical reasons: (a) sources of projection measurement error $P(R|g)$, (b) sources of projection measurement error $P(g|R)$, (c) dephasing due to leakage to intermediate state, and (d) laser noises. In the following, these error sources are discussed.

(a) The measurement error $P(g|R)$, the conditional probability of false measurement of $|g\rangle$ given that the state was initially in $|R\rangle$, mainly comes from the spontaneous emission from $|R\rangle$ to $|g\rangle$. A certain portion of Rydberg atoms, that are supposed to be absent at measurements, can be found trapped due to the spontaneous decay before escaping. Using the Rydberg atom lifetime $\tau_R = 140 \mu\text{s}$, our numerical simulation gives an estimated probability $P(g|R)$ of around 3%. Therefore, for example, the theoretical probability (solid lines) in Fig. 4 of three atoms in $|RRR\rangle$ is calculated as $P'_{RRR} = \{1 - P(g|R)\}^3 P_{RRR}$ to compare with the actual (false) measurement (data points) in Fig. 4. In addition, there are minor sources of contribution to $P(g|R)$: background atoms can enter the trap and increase $P(g|R)$, with negligibly small probability of $< 0.01\%$; coherent de-excitation from $|R\rangle$ can evolve to other ground hyperfine states due to imperfect laser polarization, which results in false $|g\rangle$ measurement of about 0.1%.

(b) The measurement error $P(R|g)$, the conditional probability of false measurement of $|R\rangle$ given that the state was initially in $|g\rangle$, is mainly caused by atoms escaping from optical tweezers, which is typically $< 3\%$ in our experiments. In addition, the atom escape probability due to background collision causes false $|R\rangle$ measurement in our experiment, estimated $< 1\%$.

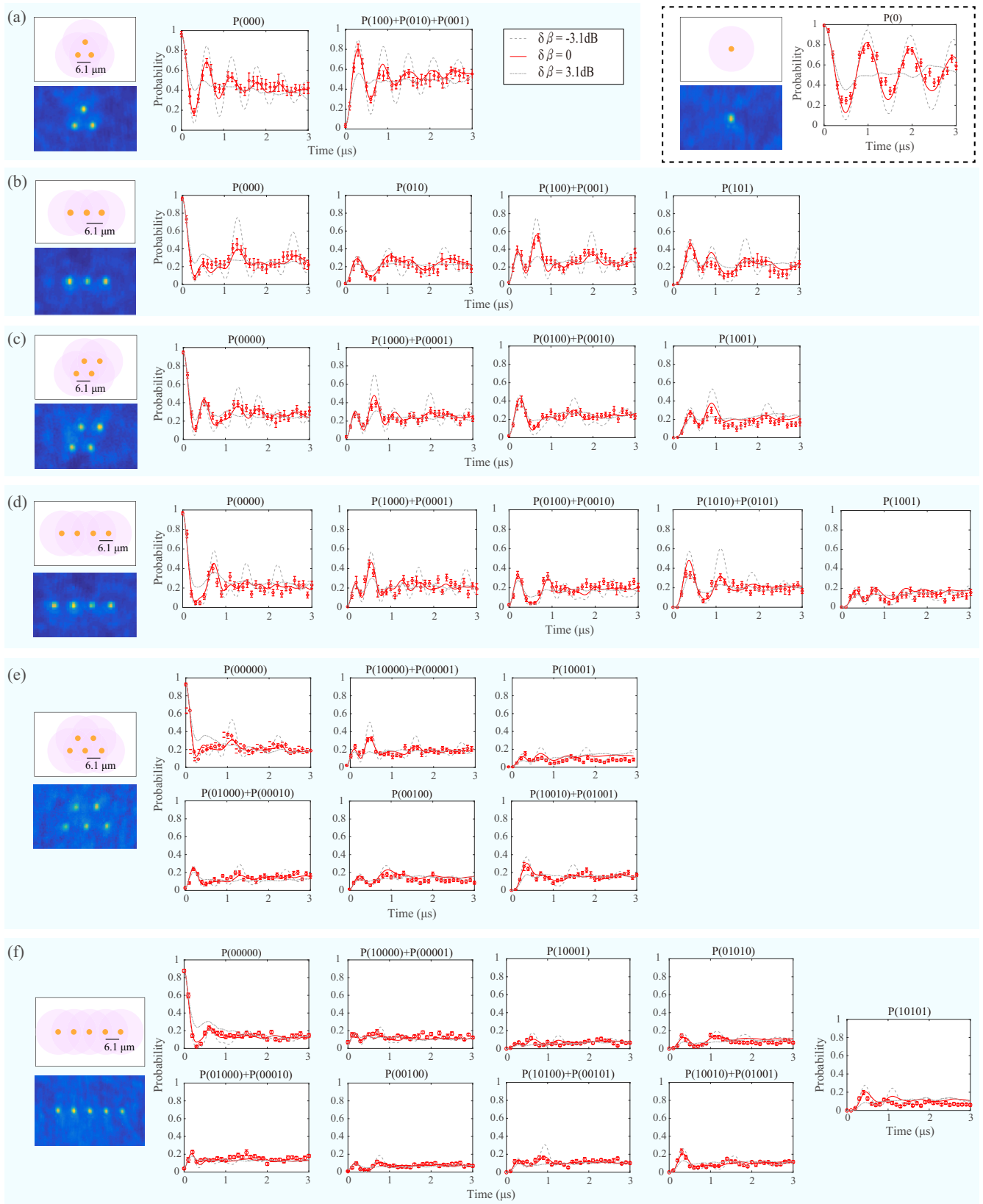


FIG. 4. (a) Triangular three ($N = 3$) atoms: geometry and image in the leftmost column, respectively, and the experimental measured probability (data points) compared to the numerical calculations for optimal fitting (solid line) and ± 3.1 dB shifts in β (dot-dashed and dashed lines), for each symmetric basis, where “0” and “1” in the states indicate $|g\rangle$ and $|R\rangle$ states, respectively. Same for the other configurations: (b) linear $N = 3$ atoms, (c) zigzag $N = 4$ atoms, (d) linear $N = 4$ atoms, (e) zigzag $N = 5$ atoms, and (f) linear $N = 5$ atoms. The inset at the top-right corner shows the single-atom case.

TABLE I. Error sources and amounts.

Error sources	
Projection measurement error $\delta P(g R)$	$\delta P = 3\%$
· Spontaneous emission $ R\rangle \rightarrow g\rangle$	$\sim 3\%$
· Background atom entering optical tweezers	$\sim 0.01\%$
· De-excitation to other ground states	$\sim 0.1\%$
Projection measurement error $\delta P(R g)$	$\delta P = 3\%$
· Atom escaping from optical tweezers	$\sim 3\%$
· Background atom collision	$\sim 1\%$
Dephasing rate	$\gamma = 1$ MHz
· Leakage to intermediate state	60 kHz
· Rydberg-excitation laser intensity noise	$\gamma_c \ll 30$ kHz
· Rydberg-excitation laser phase noise	~ 1 MHz

(c) The transition probability to the intermediate state ($|5P_{3/2}\rangle$) is nonzero during laser excitation, and the fast spontaneous decay from $|5P_{3/2}\rangle$ to $|g\rangle$ results in non-Hermitian dynamics. The leakage estimated from the detuned Rabi oscillation $\Omega_{780}^2/(\Delta_f^2 + \Omega_{780}^2) \sim 0.2\%$ is small; however, the two-level approximation [30] of the given three-level system dynamics gives the individual dephasing rate γ_{ind} in Eq. (6), which is estimated as $\sim (2\pi)20$ kHz.

(d) Rydberg excitation lasers (780 and 480 nm) have intensity and phase noises. The intensity noise is from the laser diode itself, AOM modulation error, and beam pointing error, which results in fluctuations of Ω and Δ by AC Stark shift. This fluctuation is measured as about 3% without feedback (0.7% with feedback) in our experiment, making little change in measured single-atom dynamics. The phase noise $|\Delta(f)|$ in Eq. (8), however, is estimated up to with a scaling factor, using the frequency error signals from PDH locking electronics of the lasers. All the analyses in Sec. IV are consistent with the single-atom results up to a 3-dB scaling. Note that the noise spectrum we obtained from the servo electronics might not be the same as the actual laser noise spectrum (limited by the characteristic of the photo-diode and electronics). However, it turns out that the dynamics is significantly affected by the level of noise, rather than the noise spectrum. So we focused on the consistency of the relative values of the noise levels. Also note that the phase noise we considered here is a global phase noise which applies to the all atoms homogeneously.

Further improvements of the experiment in the future can be considered as in the following. (a) The measurement error $P(g|R)$: To suppress the spontaneous decay from the Rydberg state, we can choose a higher principal or azimuthal quantum number for the Rydberg state for longer lifetime. Also, fast push-out of atoms prior to measurement by using a laser tuned for stonger repulsion of atoms can decrease the error. (b) The measurement error $P(R|g)$: This error can be reduced by improving the trap lifetime, employing enhanced atom cooling or trapping techniques [33–36]. (c) Spontaneous decay from $|5P_{3/2}\rangle$ to $|g\rangle$: This can be minimized by increasing Ω_{480} to enlarge Δ_i [30], or by using one-photon transitions with ultraviolet lights [10]. (d) Phase noises of Rydberg excitation lasers: Decreasing the phase noise requires improved locking techniques, including the technique that filters the servo bumps by using cavity-transmitting beams as excitation lasers [37–41].

VI. CONCLUSION

We present a numerical model analysis of the experimentally measured quantum few-body dynamics of Rydberg atoms. Using up to five ^{87}Rb atoms arranged in linear or zigzag configurations and excited to the Rydberg $67S$ state, we measure the time-evolving probabilities of the atomic systems in all symmetry basis. As a theoretical model, we use the Lindblad master equation for Rydberg atom chains in consideration of experimental error sources, such as the projection measurement errors, the leakage to an intermediate state, and the phase noise of the excitation lasers. The resulting calculation agreed well with the experimentally observed measurements, suggesting that the quantum dynamics of Rydberg-atom systems are suitably described with the current model extending the single-body dephasing model [30] to a few-body problem.

ACKNOWLEDGMENTS

This research was supported by Samsung Science and Technology Foundation [SSTF-BA1301-12], National Research Foundation of Korea (NRF) (2017R1E1A1A01074307), and the Institute for Information & communications Technology Promotion (IITP-2018-2018-0-01402).

-
- [1] H. J. Briegel, T. Calarco, D. Jaksch, J. I. Cirac, and P. Zoller, Quantum computing with neutral atoms, *J. Mod. Opt.* **47**, 415 (2000).
- [2] I. H. Deutsch, G. K. Brennen, and P. S. Jessen, Quantum computing with neutral atoms in an optical lattice, *Fortschr. Phys.* **48**, 925 (2000).
- [3] M. Saffman, Quantum computing with atomic qubits and Rydberg interactions: progress and challenges, *J. Phys. B: At., Mol. Opt. Phys.* **49**, 202001 (2016).
- [4] C. Gross and I. Bloch, Quantum simulations with ultracold atoms in optical lattices, *Science* **357**, 995 (2017).
- [5] I. I. Ryabtsev, D. B. Tretyakov, and I. I. Beterov, Applicability of Rydberg atoms to quantum computers, *J. Phys. B: At., Mol. Opt. Phys.* **38**, S421 (2005).
- [6] N. Schlosser, G. Reymond, and P. Grangier, Collisional Blockade in Microscopic Optical Dipole Traps, *Phys. Rev. Lett.* **89**, 023005 (2002).
- [7] Z. Zuo, M. Fukusen, Y. Tamaki, T. Watanabe, Y. Nakagawa, and K. Nakagawa, Single atom Rydberg excitation in a small dipole trap, *Opt. Express* **17**, 22898 (2009).
- [8] E. Urban, T. A. Johnson, T. Henage, L. Isenhower, D. D. Yavuz, T. G. Walker, and M. Saffman, Observation of Rydberg blockade between two atoms, *Nat. Phys.* **5**, 110 (2009).
- [9] T. Wilk, A. Gaetan, C. Evellin, J. Wolters, Y. Miroshnychenko, P. Grangier, and A. Browaeys, Entanglement of two individual Neutral Atoms Using Rydberg Blockade, *Phys. Rev. Lett.* **104**, 010502 (2010).

- [10] Y. Y. Jau, A. M. Hankin, T. Keating, I. H. Deutsch, and G. W. Biedermann, Entangling atomic spins with a Rydberg-dressed spin-flip blockade, *Nat. Phys.* **12**, 71 (2016).
- [11] L. Isenhower, E. Urban, X. L. Zhang, A. T. Gill, T. Henage, T. A. Johnson, T. G. Walker, and M. Saffman, Demonstration of a Neutral atom Controlled-NOT Quantum Gate, *Phys. Rev. Lett.* **104**, 010503 (2010).
- [12] K. M. Maller, M. T. Lichtman, T. Xia, Y. Sun, M. J. Piotrowicz, A. W. Carr, L. Isenhower, and M. Saffman, Rydberg-blockade controlled-not gate and entanglement in a two-dimensional array of neutral-atom qubits, *Phys. Rev. A* **92**, 022336 (2015).
- [13] F. Nogrette, H. Labuhn, S. Ravets, D. Barredo, L. Béguin, A. Vernier, T. Lahaye, and A. Browaeys, Single-Atom Trapping in Holographic 2D Arrays of Microtraps with Arbitrary Geometries, *Phys. Rev. X* **4**, 021034 (2014).
- [14] W. Lee, H. Kim, and J. Ahn, Three-dimensional rearrangement of single atoms using actively controlled optical microtraps, *Opt. Exp.* **24**, 9816 (2016).
- [15] H. Kim, W. Lee, H.-G. Lee, H. Jo, Y. Song, and J. Ahn, In situ single-atom array synthesis by dynamic holographic optical tweezers, *Nat. Commun.* **7**, 13317 (2016).
- [16] D. Barredo, S. de Léséleuc, V. Lienhard, T. Lahaye, and A. Browaeys, An atom-by-atom assembler of defect-free arbitrary 2d atomic arrays, *Science* **354**, 1021 (2016).
- [17] M. Endres, H. Bernien, A. Keesling, H. Levine, E. R. Anschuetz, A. Krajenbrink, and M. D. Lukin, Atom-by-atom assembly of defect-free one-dimensional cold atom arrays, *Science* **354**, 1024 (2016).
- [18] D. Barredo, V. Lienhard, S. de Léséleuc, T. Lahaye, and A. Browaeys, Synthetic three-dimensional atomic structures assembled atom by atom, *Nature* **561**, 79 (2018).
- [19] A. Kumar, T.-Y. Wu, F. Giraldo, and D. S. Weiss, Sorting ultracold atoms in a three-dimensional optical lattice in a realization of Maxwell's demon, *Nature* **561**, 83 (2018).
- [20] H. Labuhn, D. Barredo, S. Ravets, S. De Léséleuc, T. Macrì, T. Lahaye, and A. Browaeys, Tunable two-dimensional arrays of single Rydberg atoms for realizing quantum Ising models, *Nature* **534**, 667 (2016).
- [21] H. Bernien, S. Schwartz, A. Keesling, H. Levine, A. Omran, H. Pichler, S. Choi, A. S. Zibrov, M. Endres, M. Greiner, V. Vuletić, and M. D. Lukin, Probing many-body dynamics on a 51-atom quantum simulator, *Nature* **551**, 579 (2017).
- [22] S. de Léséleuc, V. Lienhard, P. Scholl, D. Barredo, S. Weber, N. Lang, H. P. Büchler, T. Lahaye, and A. Browaeys, Experimental realization of a symmetry protected topological phase of interacting bosons with Rydberg atoms, [arXiv:1810.13286](https://arxiv.org/abs/1810.13286).
- [23] H. Kim, Y. J. Park, K. Kim, H. S. Sim, and J. Ahn, Detailed Balance of Thermalization dynamics in Rydberg-atom Quantum simulators, *Phys. Rev. Lett.* **120**, 180502 (2018).
- [24] H. Weimer, M. Müller, I. Lesanovsky, P. Zoller, and H. P. Büchler, A Rydberg quantum simulator, *Nat. Phys.* **6**, 382 (2010).
- [25] L. Béguin, A. Vernier, R. Chicireanu, T. Lahaye, and A. Browaeys, Direct Measurement of the van der Waals Interaction Between two Rydberg Atoms, *Phys. Rev. Lett.* **110**, 263201 (2013).
- [26] M. D. Lukin, M. Fleischhauer, R. Cote, L. M. Duan, D. Jaksch, J. I. Cirac, and P. Zoller, Dipole Blockade and Quantum information Processing in Mesoscopic Atomic Ensembles, *Phys. Rev. Lett.* **87**, 037901 (2001).
- [27] E. Braaten, H. W. Hammer, and G. P. Lepage, Lindblad equation for the inelastic loss of ultracold atoms, *Phys. Rev. A* **95**, 012708 (2017).
- [28] G. Lindblad, On the generators of quantum dynamical semigroups, *Commun. Math. Phys.* **48**, 119 (1976).
- [29] V. Gorini, A. Kossakowski, and E. C. G. Sudarshan, Completely positive dynamical semigroups of N-level systems, *J. Math. Phys.* **17**, 821 (1976).
- [30] S. de Léséleuc, D. Barredo, V. Lienhard, A. Browaeys, and T. Lahaye, Analysis of imperfections in the coherent optical excitation of single atoms to Rydberg states, *Phys. Rev. A* **97**, 053803 (2018).
- [31] W. Lee, H. Kim, and J. Ahn, Defect-free atomic array formation using the Hungarian matching algorithm, *Phys. Rev. A* **95**, 053424 (2017).
- [32] I. I. Ryabtsev, I. I. Beterov, D. B. Tretyakov, V. M. Entin, and E. A. Yakshina, Spectroscopy of cold rubidium Rydberg atoms for applications in quantum information, *Phys.-Uspekhi* **59**, 196 (2016).
- [33] H. J. Lee, C. S. Adams, M. Kasevich, and S. Chu, Raman Cooling of Atoms in an Optical Dipole Trap, *Phys. Rev. Lett.* **76**, 2658 (1996).
- [34] P. Xu, X. He, J. Wang, and M. Zhan, Trapping a single atom in a blue detuned optical bottle beam trap, *Opt. Lett.* **35**, 2164 (2010).
- [35] A. M. Kaufman, B. J. Lester, and C. A. Regal, Cooling a Single Atom in an Optical Tweezer to Its Quantum Ground State, *Phys. Rev. X* **2**, 041014 (2012).
- [36] P. A. Willems and K. G. Libbrecht, Creating long-lived neutral-atom traps in a cryogenic environment, *Phys. Rev. A* **51**, 1403 (1995).
- [37] J. Hald and V. Ruseva, Efficient suppression of diode-laser phase noise by optical filtering, *J. Opt. Soc. Am. B* **22**, 2338 (2005).
- [38] T. Nazarova, C. Lisdat, F. Riehle, and U. Sterr, Low-frequency-noise diode laser for atom interferometry, *J. Opt. Soc. Am. B* **25**, 1632 (2008).
- [39] N. Akerman, N. Navon, S. Kotler, Y. Glickman, and R. Ozeri, Universal gate-set for trapped-ion qubits using a narrow linewidth diode laser, *New J. Phys.* **17**, 113060 (2015).
- [40] L. Gerster, Spectral filtering and laser diode injection for multi-qubit trapped ion gates, Master's thesis, ETH Zurich, 2015.
- [41] H. Levine, A. Keesling, A. Omran, H. Bernien, S. Schwartz, A. S. Zibrov, M. Endres, M. Greiner, V. Vuletić, and M. D. Lukin, High-Fidelity Control and Entanglement of Rydberg-Atom Qubits, *Phys. Rev. Lett.* **121**, 123603 (2018).